© 2020. Published by The Company of Biologists Ltd | Journal of Experimental Biology (2020) 223, jeb218552. doi:10.1242/jeb.218552

RESEARCH ARTICLE

Maximum aerodynamic force production by the wandering glider dragonfly (*Pantala flavescens*, Libellulidae)

Guanting Su[1,2], Robert Dudley[2,3], Tianyu Pan[1,*], Mengzong Zheng[1], Liansong Peng[1] and Qiushi Li[1,4]

ABSTRACT

Maximum whole-body force production can influence behavioral outcomes for volant taxa, and may also be relevant to aerodynamic optimization in microair vehicles. Here, we describe a new method for measuring maximum force production in free-flying animals, and present associated data for the wandering glider dragonfly. Flight trajectories were repeatedly acquired from pull-up responses by insects dropped in mid-air with submaximal loads attached beneath the center of body mass. Forces were estimated from calculations of the maximum time-averaged acceleration through time, and multiple estimates were obtained per individual so as to statistically facilitate approximation of maximum capacity through use of the Weibull distribution. On a group level, wandering glider dragonflies were here estimated to be capable of producing total aerodynamic force equal to ∼4.3 times their own body weight, a value which significantly exceeds earlier estimates made for load-lifting dragonflies, and also for other volant taxa in sustained vertical load-lifting experiments. Maximum force production varied isometrically with body mass. Falling and recovery flight with submaximal load represents a new context for evaluating limits to force production by flying animals.

KEY WORDS: Allometry, Flight, Load lifting, Maximum performance, Trajectory kinematics

INTRODUCTION

Limits to maximum flight performance may derive independently from anatomical, physiological and aerodynamic constraints on animals, or from their interactions. Experimental manipulations of wing shape (e.g. Vance and Roberts, 2014; Ray et al., 2016) and wing flexibility (e.g. Mountcastle and Combes, 2013), along with hypobaric and hypodense gas manipulations (e.g. Chai and Dudley, 1995; Chai and Dudley, 1996), have demonstrated various limiting factors on force and power production for a number of volant taxa. Such studies may also inform engineering applications, e.g. optimization of aerodynamic forces generated by the wings of microair vehicles. Maximum whole-body force was recognized early on as potentially indicative of limits to animal flight performance (see Plateau, 1865), and has often been studied via vertical load-lifting assays given that the majority of resultant forces during flight act to offset gravity (see Marden, 1987; Dudley, 2000).

[1]National Key Laboratory of Science and Technology on Aero-Engine Aero-Thermodynamics, School of Energy and Power Engineering, Beihang University, Beijing 100191, China. [2]Department of Integrative Biology, University of California, Berkeley, Berkeley, CA 94720, USA. [3]Smithsonian Tropical Research Institute, Balboa, Republic of Panama. [4]Key Laboratory of Fluid and Power Machinery, Xihua University, Chengdu 610039, China.

*Author for correspondence (pantianyu@buaa.edu.cn)

G.S., 0000-0002-1295-9599; T.P., 0000-0002-9158-8262

Received 18 November 2019; Accepted 19 May 2020

Dragonflies (Odonata: Anisoptera) are fast and agile insect fliers, and are known to exhibit free-flight accelerations as high as ∼40 m s^{-2} (Bomphrey et al., 2016; May, 1991; Rüppell, 1989; Lohmann et al., 2019). Marden (1987) cumulatively applied abdominal loads to 29 individual dragonflies from six different species, and derived maximum vertical forces averaging about 2.8 times the body weight. Methodological constraints associated with cumulative load lifting may, however, have resulted in underestimates of the maximum capacity for force production (see Dudley, 2000; Buchwald and Dudley, 2010). An alternative asymptotic load-lifting method was developed by Chai et al. (1997) for hummingbirds and later modified for orchid bees (Dillon and Dudley, 2004), bumblebees (Buchwald and Dudley, 2010) and tree sparrows (Sun et al., 2016), and has enabled detailed studies of allometric and ecological variability in the maximum vertical forces produced by animal fliers. However, our preliminary application of the asymptotic load-lifting method to dragonflies yielded erratic behaviors and non-vertical flight trajectories.

Instead, here we applied a newly developed experimental protocol to the wandering glider dragonfly (*Pantala flavescens*), a species renowned for extraordinary feats of flight, including transoceanic migrations (Anderson, 2009) and occurrence at the particularly high elevation of 6300 m in the Himalayas (Corbet, 2004). The experimental protocol involved the dropping in mid-air of dragonflies to which were attached a range of submaximal loads, followed by tracking of the ensuing trajectory. We then estimated time-averaged aerodynamic forces produced by the insects during this loaded fall and their subsequent ascent using acceleration estimates as extracted from the flight trajectory. We hypothesized that sustained forces elicited from these lifting trajectories would exceed those obtained in earlier cumulative load-lifting evaluations of dragonflies (Marden, 1987), and also that free-flight responses to load (and potential motivating cues of optomotor slip) might elicit the generation of weight-specific forces exceeding those recorded for other insects of comparable body mass in asymptotic load lifting. We also obtained repeated measures of performance per individual, and used Weibull distribution modeling (Hagey et al., 2016) to better estimate individual lifting capacity.

MATERIALS AND METHODS

Dragonflies, *Pantala flavescens* (Fabricius 1798), were captured on the main campus of Beihang University (Beijing, Peoples Republic of China) from 3 to 10 August 2018, and were used in experiments on the day of capture. The male/female ratio of the study population was approximately 3:2, but we pooled data from the two sexes to obtain a species-level assay of maximum performance. Following hypothermic anesthetization of individual dragonflies (Li et al., 2018), body mass and wing morphological parameters (Table S1) were measured. For each individual dragonfly, a small globule of melted soldering tin was then glued onto the ventral segment of the metepimeron nominally beneath the center of body mass of the

Journal of Experimental Biology (2020) 223, jeb218552. doi:10.1242/jeb.218552

List of symbols and abbreviations

a_H	horizontal acceleration
a_V	vertical acceleration
a_{x2}	time-averaged *X*-accelerations during forward phase
a_{y2}	time-averaged *Y*-accelerations during forward phase
a_{z3}	time-averaged *Z*-accelerations during pull-up phase
C_r	recovery coefficient
d.f.	degrees of freedom
F_H	horizontal aerodynamic force produced accompanying the production of F_V
F^*_H	body weight-specific horizontal aerodynamic force accompanying the production of F_V
F_{max}	individual maximum aerodynamic force production
F^*_{max}	individual maximum body weight-specific aerodynamic force production
F_V	maximum vertical aerodynamic force produced during a single flight
F^*_V	maximum body weight-specific vertical aerodynamic force produced during a single flight
F^*_X, F^*_Y and F^*_Z	*X*-, *Y*- and *Z*-component of body weight-specific aerodynamic force, respectively
g	gravitational acceleration (–9.8 m s^{-2})
m_b	initial body mass of dragonfly
m_l	mass of globule (load)
N	number of individuals/sample size
QCA	quasi-constant acceleration
R	loading ratio
t	time after release
T	time period of dragonfly's acceleration from w_{min} to w_{max}
u, v and w	*X*-, *Y*- and *Z*-velocity, respectively
w_{max}	dragonfly's maximum vertical velocity after upward acceleration
w_{min}	dragonfly's minimum vertical velocity during the flight
x, y and z	*X*-, *Y*- and *Z*-position, respectively
(X, Y, Z)	global coordinate system
λ	scale parameter of Weibull distribution model

insect (Fig. 1; Li et al., 2018). The mass of each globule (m_l) was specified as a ratio relative to the initial mass of the dragonfly (m_b); values for this loading ratio R=m_l/m_b of 1.0 (N=1), 1.2 (N=3), 1.5 (N=19) and 1.8 (N=7) were used in experiments, and were assigned haphazardly to individual dragonflies. Loads greater than 1.8 times the body mass were not used because preliminary trials (N=5) found no individual that could offset a load twice their body mass during loaded fall after being dropped from rest. In experiments, each dragonfly (within several minutes of morphological measurements) was held by its four wings as folded dorsally, was lifted near the top of the flight chamber, and was then dropped at a nominally horizontal body orientation so as to initiate the loaded fall (Fig. 1; Movies 1 and 2). For filming, only individuals with intact wings and no obvious body damage were used. Two orthogonally arranged cameras (operated at 500 frames s^{-1}) were used to film flight trajectories within an open-top glass cube (volume of 0.6 m^3; 0.8 m×0.8 m×1.0 m), using a configuration identical to that of Li et al. (2018). Vertical coverage of the two cameras was restricted to regions at least 0.3 m above the cube's floor, thereby excluding filming of any flights that potentially would invoke the ground effect. Following initial filming, additional trials were performed (with 3 min resting periods between flight events) up to the time when insects failed to sustain body weight during flight. During filming, air temperature inside the experimental chamber was ∼36°C. Before filming and in between trials, dragonflies were housed in mesh cages at ambient air temperature, which was typically 30°C.

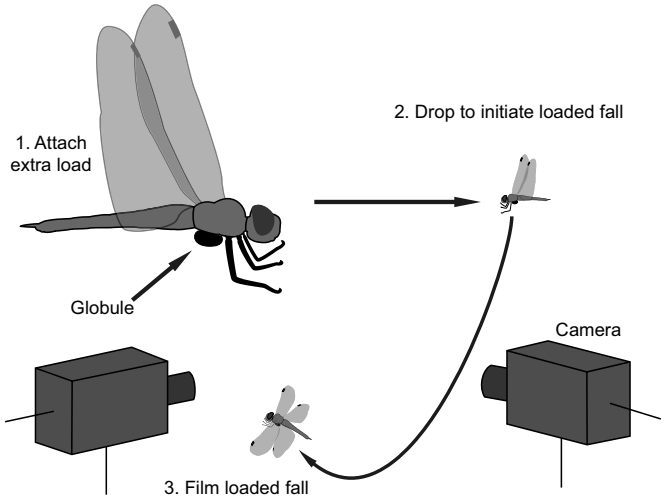

Fig. 1. Experimental procedure. For details, see Materials and Methods.

Pixel coordinates approximating the position of the dragonfly's center of mass during flight were tracked using DLTdv5 digitizing tool (Hedrick, 2008) operating in Matlab (8.3.0.532, R2014a). Using the same three-dimensional reconstruction algorithm as in Li et al. (2018), time series of the pixel coordinates were converted to a global (X, Y, Z) coordinate system in which the positive direction of the Z-axis was defined as vertically upward (see Li et al., 2018), the Y-axis was generally aligned with the dragonfly's sagittal plane anteriorly when initially dropped, and the X-axis pointed in the right lateral direction of the dragonfly. Positional data were then smoothed using a quintic spline filter with the low-pass cut-off frequency specified as 20 Hz, which was approximately the lower limit of dragonfly's wing flapping frequency during the loaded fall. Root mean square level of the removed noise was around 0.7 mm, and smoothed positional data were differentiated to produce time series of velocity vectors (see Fig. S1). The aforementioned data processing procedure was completed using the GCVSPL package (https://isbweb.org/software/sigproc.html; Woltring, 1986). We then identified sufficiently long time periods during which acceleration was relatively constant, here termed quasi-constant acceleration (QCA). Two criteria were used to identify periods of QCA; one was the absolute value of the Pearson correlation coefficient between a velocity component and time over sample periods, for which we set the high-pass threshold to be 0.99. As revealed by the flight trajectory kinematics (see Results and Table 1), dragonflies produced maximum aerodynamic force over a time period of approximately 150 ms. Therefore, we chose a minimum period length of 150 ms (corresponding to 3–5 wingbeats; see Li et al., 2018; Wakeling and Ellington, 1997); both aforementioned criteria were necessary for classification as a

Table 1. Estimated body weight-specific aerodynamic force

	Free-fall	Forward	Pull-up	Recovery
F^*_X	0.0	0.5	∼0.0	−0.1
F^*_Y	0.0	2.2	∼0.0	−1.4
F^*_Z	0.5	∼2.5	4.2	3.2
F^*_R	0.5	3.4	4.2	3.5

Data were derived from slopes of the averaged velocity curves during the corresponding time interval for each of the four flight phases, including force components along the *X*-, *Y*- and *Z*-axes (F^*_X, F^*_Y and F^*_Z, respectively) and the resultant force (F^*_R); see Results for further explanation.

Journal of Experimental Biology (2020) 223, jeb218552. doi:10.1242/jeb.218552

QCA period (see Fig. 2). All such periods used for analysis corresponded to at least 76 video frames in duration. Linear equations were fitted using ordinary least squares regressions to the velocity–time curves within QCA periods. The slope of each regression was used as an estimate of the time-averaged acceleration for the corresponding QCA period; time-averaged accelerations for all QCA periods were then compared to obtain the dragonfly's maximum time-averaged acceleration along a coordinate axis during the entire flight (Fig. 2).

Maximum aerodynamic force production was calculated based on time-averaged accelerations, such that vertical force F_V and horizontal force F_H were estimated as:

$$F_V = (m_b + m_l) \cdot (a_V - g), \quad (1)$$

$$F_H = (m_b + m_l) \cdot a_H, \quad (2)$$

where a_V and a_H are vertical and horizontal acceleration, respectively, and g is gravitational acceleration (-9.8 m s^{-2}). We also expressed body weight-specific force in the vertical and horizontal directions, F_V^* and F_H^*, respectively, using the following equations:

$$F_V^* = \frac{F_V}{|m_b g|} = (1 + R) \cdot \left(\frac{a_V - g}{|g|} \right), \quad (3)$$

$$F_H^* = \frac{F_H}{|m_b g|} = (1 + R) \cdot \frac{a_H}{|g|}. \quad (4)$$

We then estimated group-level maximum performance from multiple observations on different individuals (see Hagey et al., 2016, 2017). First, individual maximum capacity based on repeated measures of maximum performance was determined, using Weibull distribution modeling, which substantially reduces the influence of rare observations (see Hagey et al., 2016). For individuals for which maximum force production was evaluated multiple times, maximum capacity was equated to the scale parameter (λ) of the Weibull distribution model, and the estimation error was equated to the standard error of λ. For individuals with only one observation, individual maximum capacity was assumed to equal that of this single performance. Species-level maximum capacity was then estimated as the average of multiple individual capacities (as weighted by their corresponding estimation errors), thus minimizing effects of either small sample sizes for particular individuals or large variation among trials (Hagey et al., 2016). Data from individuals with only one observation were excluded when estimating species-level capacity. Weibull distribution modeling was performed using Matlab (8.3.0.532, R2014a); other statistical tests, e.g. Student's *t*-tests, were performed using R (3.5.2).

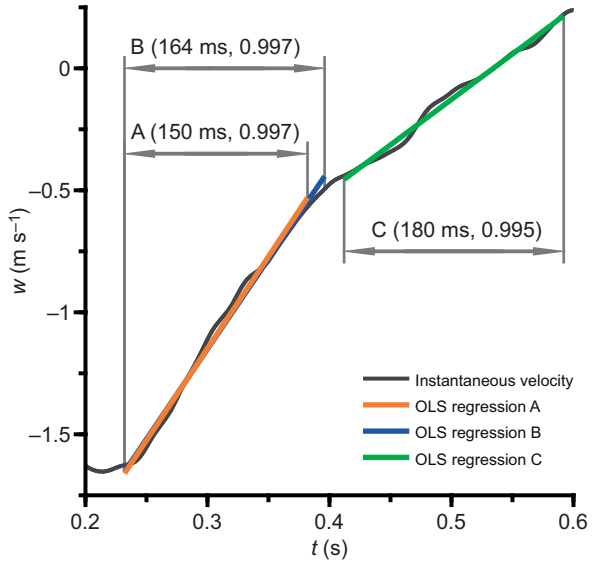

Fig. 2. Three representative quasi-constant acceleration (QCA) periods (A–C) for a vertical velocity time series of one loaded fall trial. Trial index: 1808091348; performing individual index: 180809-4; *t*=0, time of release; *w*, *Z*-velocity. Each period is labeled in the format: period index (duration of period, Pearson correlation coefficient between vertical velocity and time over the period). Results of ordinary least squares linear regressions for each of the three periods are as follows: A, *w*=7.53 *t*–3.41 (*P*<0.001); B, *w*=7.38 *t*–3.36 (*P*<0.001); C, *w*=3.72 *t*–1.99 (*P*<0.001). Different QCA periods may partially overlap in time, and may even start or end at the same time instant (e.g. A and B). Assuming that A, B and C are the only QCA periods for this trial (given the vertical velocity curve), maximum time-averaged vertical acceleration during this flight was estimated to be 7.53 m s^{-2}.

RESULTS

Trajectory kinematics

Thirty individuals were filmed in experiments, from which complete trajectories were obtained for 143 loaded falls (referred to as full-trajectory trials; see Fig. 3; Fig. S2 and Table S2). An additional 35 trials were filmed which omitted the initial descent, referred to here as partial-trajectory trials (Table S2). Data from partial-trajectory trials were not included in the graphical illustration of the results (i.e. Figs 3 and 4), but were used to evaluate maximum acceleration. Typically, falling individuals locomoted downward and forward as in diving flight, followed by a pull-up (Fig. 3). Dragonflies veered haphazardly to the left and right when falling (Figs 3 and 4A), but showed generally consistent trends in downward and forward motions (Fig. 4C,E) and in associated speeds (Fig. 4D,F).

Four different temporal phases of the trajectory were identified based on overall trends in the velocity curves. A free-fall phase (0–0.10 s after the drop; phase I in Fig. 4) was marked by rapid increases in the dragonfly's falling speed, but with relatively small

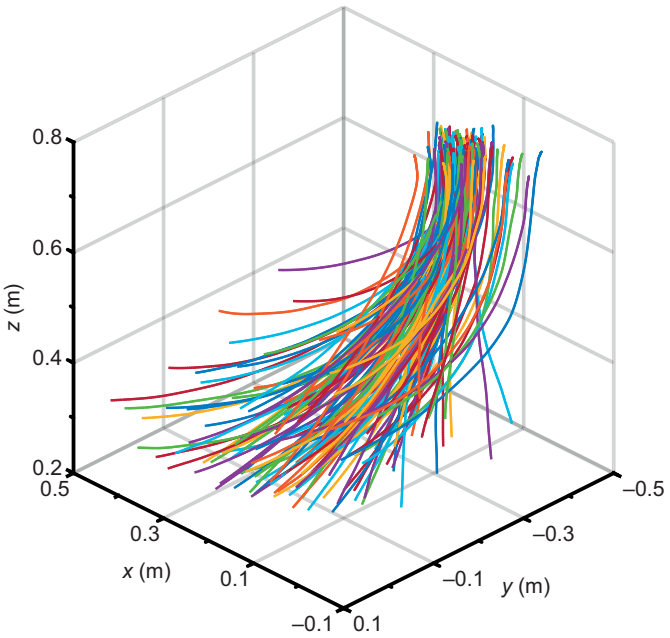

Fig. 3. Three-dimensional flight trajectories (up to the moment of positive vertical velocity) from 143 full-trajectory trials. Trajectory regions following acquisition of positive vertical velocity are not plotted to avoid visual clutter.

Journal of Experimental Biology (2020) 223, jeb218552. doi:10.1242/jeb.218552

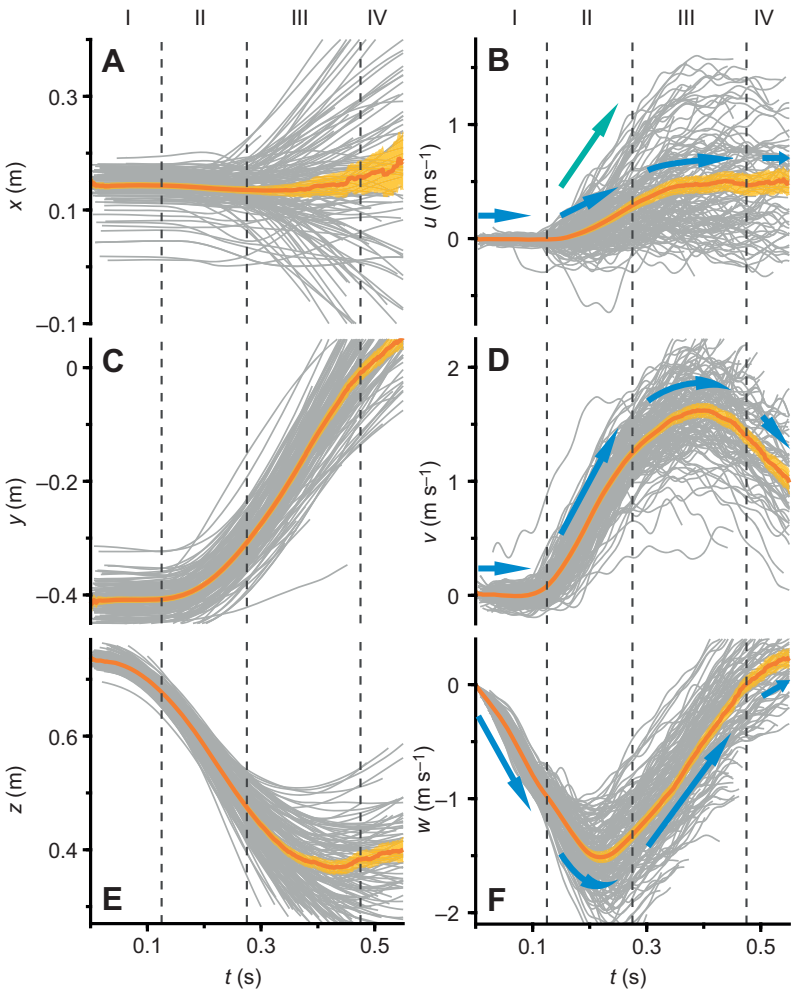

Fig. 4. Time series data for the 143 full-trajectory trials. (A) *x*, *X*-position after release (*t*=0, time of release). (B) *u*, *X*-velocity after release; for trials in which dragonflies turned laterally to their left, velocity data for an axisymmetrically mirrored lateral motion on their right are instead shown. (C) *y*, *Y*-position after release. (D) *v*, *Y*-velocity after release. (E) *z*, *Z*-position after release. (F) *w*, *Z*-velocity after release. In A–F, thin gray lines indicate separate flight sequences; amber lines and shaded areas correspond to the mean value and 95% confidence intervals, respectively; the three vertical dashed lines (located at *t*=0.125 s, 0.275 s and 0.475 s, respectively) indicate the approximate periods for the four phases of the trajectories, each of which is marked by a Roman numeral. In B, D and F, blue arrows emphasize the overall trend for the average velocity curve during these phases. Slopes of some *u*-curves exhibited a large discrepancy with averaged *u*-curve during the forward phase, and the green arrow in B emphasizes the typical slope for some of these curves during the forward phase.

variation in horizontal speed. Right after the drop, the falling speed of the dragonfly increased rapidly to 1–2 m s^{-1} (Fig. 4F). From 0 to 0.10 s after the drop, the vertical velocity curves exhibited a mean slope of −7.9 m s^{-2}, suggesting that acceleration during this phase was mainly due to gravity with no significant aerodynamic force production.

Then, a forward phase of the flight (0.15–0.25 s; phase II in Fig. 4) was marked by a rapid and consistent increase in the dragonfly's forward velocity (up to ∼2 m s^{-1}; Fig. 4D), accompanied by an increase in the vertical acceleration, as indicated by convexity in the vertical velocity curves (Fig. 4F). *X*-velocity curves exhibited a generally upward trend, but with substantial variation among separate trials. During this forward phase, dragonflies in most trials reached their minimum vertical speed. From 0.15 to 0.25 s after the drop, the averaged *X*-velocity and *Y*-velocity curves exhibited a mean slope of 2.1 m s^{-2} and 8.6 m s^{-2}, respectively. Dragonflies maintained a high horizontal force in this phase to effect forward acceleration, along with increased vertical force production.

During a pull-up phase (0.3–0.45 s; phase III in Fig. 4), vertical velocity rapidly increased concomitantly with reductions in horizontal acceleration. Vertical velocity curves also showed reduced convexity (Fig. 4F), suggesting positive and more constant accelerations compared with those in the forward phase of the flight. The mean slope of the averaged *Z*-velocity curve from 0.3 to 0.45 s after the drop was 6.8 m s^{-2}, while vertical velocity approached zero (Fig. 4F). Dragonflies thus produced high and sustained vertical forces in parallel with decreased horizontal force.

In the final recovery phase (0.50–0.55 s; phase IV in Fig. 4), when the falling speed of the dragonfly approached zero, vertical and horizontal accelerations simultaneously decreased relative to those in the pull-up phase. From 0.50 to 0.55 s after the drop, the mean slope of the averaged *Y*-velocity and *Z*-velocity curves decreased to −5.6 m s^{-2} and 2.7 m s^{-2}, respectively, indicating reduced vertical force output and slowed forward motion.

In some trials, dragonflies exhibited time-averaged *X*-accelerations as high as 9 m s^{-2} during the forward phase (see Fig. 4B, green arrow). For all full-trajectory trials, we calculated time-averaged *X*- and *Y*-accelerations during the forward phase, denoted as a_{x2} and a_{y2}, respectively. The corresponding magnitudes of horizontal acceleration, $\sqrt{a_{x2}^2 + a_{y2}^2}$, were all less than 13.5 m s^{-2} (Fig. 5). Also, there was a complementary relationship between the square of a_{x2} and that of a_{y2}, as indicated by a significant linear regression between these data points whenever the magnitude of horizontal acceleration exceeded 9 m s^{-2} (see Fig. 5). This result suggests that, rather than being associated with an independent lateral motion, *X*-accelerations simply resulted from a reorientation of the total force vector.

To summarize the general features of these loaded fall trajectories, dragonflies underwent large anterior accelerations following an initial period of free fall. After rapid anterior

Journal of Experimental Biology (2020) 223, jeb218552. doi:10.1242/jeb.218552

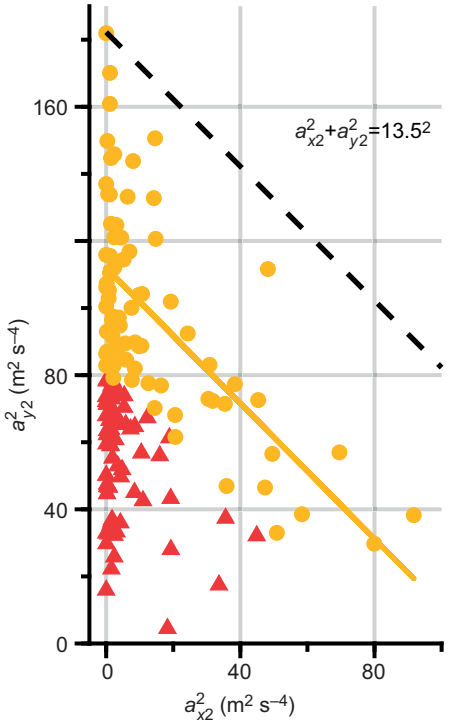

Fig. 5. Relationship between the squared time-averaged values of *Y*-acceleration and *X*-acceleration during the forward phase for the 143 full-trajectory trials. Data points with $a_{x2}^2+a_{y2}^2<81$ are indicated by red triangles, and other points exceeding this value are indicated by orange circles ($a_{y2}^2=112-1.01a_{x2}^2$, r^2=0.41, P<0.001). The black dashed line marks the upper limit of $a_{x2}^2+a_{y2}^2$ (=13.5^2).

acceleration, falling speed then tended to decline as a result of increased and sustained vertical force production.

Maximum force production in single flights

The magnitude and direction of time-averaged aerodynamic force production during the four phases were first estimated from slopes of the averaged velocity curves during corresponding time intervals. For a loading ratio (R) of 1.5 (the value most frequently used in this study), body weight-specific force components and the resultant total force during the four phases were calculated (Table 1). Time-averaged Z-acceleration during the forward phase, and X- and Y-accelerations during the pull-up phase, were assumed to be zero, given convexity in the associated sections of the velocity curves (see Fig. 4D,F).

Moreover, to account for the aforementioned discrepancy between individual X-velocity curves and the averaged X-velocity curve during the forward phase of some trials, we compared time-averaged aerodynamic force production during the forward phase with force production during the pull-up phase for each separate flight. We calculated time-averaged Z-acceleration (a_{z3}) during the pull-up phase for 102 full-trajectory trials (duration of the other 41 trials being less than 0.45 s), and obtained each trial's body weight-specific resultant force production during the two phases, $(1+R)/|g|\cdot\|(a_{x2},a_{y2},-g)\|$ and $(1+R)/|g|\cdot\|(0,0,a_{z3}-g)\|$, respectively. A paired bi-directional Student's t-test (P<0.001) demonstrated that dragonflies significantly generated 15% more body weight-specific force (difference of mean body weight-specific force of 0.49, 95% confidence interval: 0.41–0.58) during the pull-up phase relative to the forward phase.

Consequently, the greatest resultant force was produced in the pull-up phase (among the four trajectory phases), and its direction was generally aligned vertically (Table 1). Using the QCA method, we calculated maximum vertical acceleration for 148 trials derived from 30 individuals (consisting of 121 full-trajectory trials from 25 individuals, and 27 partial-trajectory trials from 11 individuals; partial-trajectory trials contained the pull-up phases for maximum vertical acceleration calculations). The other 30 trials of the 178 total trials lacked appropriate QCA periods to calculate maximum force and were not included in the analysis (see Discussion). Corresponding maximum vertical forces F_V averaged 1.41×10^{-2} N (s.d. of 3.0×10^{-3} N), and their body weight-specific values F_V^* averaged 4.18 (s.d. of 0.58), with the highest value being 5.81. Horizontal forces produced during the pull-up phase could not be accurately calculated using the QCA method because of considerable variation in X- and Y-accelerations (see Fig. 4B,D). Nonetheless, horizontal forces were approximated for each trial by time-averaging components of horizontal acceleration over the same QCA period. Horizontal forces F_H during these periods averaged 3.3×10^{-3} N (s.d. of 1.9×10^{-3} N), and body weight-specific values F_H^* averaged 0.99 (s.d. of 0.52), corresponding to ∼24% of the vertical force and with the highest value being 2.54. There was a non-significant linear relationship between horizontal and vertical forces ($F_H^*=0.13F_V^*+0.43$, r^2=0.02, P=0.07).

Combining these maximum vertical force estimates with the corresponding horizontal forces, the total aerodynamic force was calculated as their resultant. For the 148 trials, total force exceeded the maximum vertical force only by small amounts (average of 4%, with a maximum of 18%). Given their small contribution to total force as well as their much lower accuracy of estimation, all horizontal forces were subsequently neglected and the vertical force was considered to represent the total force output.

Maximum force production by individuals, and group-level capacity

Neglecting innate individual differences, two external factors (i.e. the loading ratio and the categorical variable as to whether or not the start of the loaded fall trajectory was recorded) were considered to evaluate associated effects on estimates of individual maximum performance. Individual maximum body weight-specific force production (F_{max}^*), as determined using Weibull distribution modeling for multiple-observation individuals, was used to compare individuals of different body mass.

For the 143 full-trajectory trials, maximum vertical force production was obtained using the QCA method from 121 trials by 25 individuals (multiple-observation individuals, N=18), for which F_{max}^* was then determined. These values of F_{max}^* were then segregated into three groups according to their loading ratio [i.e. R=1.0 or 1.2 (N=4), R=1.5 (N=15) and R=1.8 (N=6)], and unpaired bi-directional Student's t-tests were employed to detect differences among groups (Table 2). F_{max}^* of individuals with an R of 1.5 did not significantly differ from those with an R of 1.8, whereas individuals with an R of 1.0 or 1.2 exhibited significantly lower values of F_{max}^* when compared with the other two groups with higher R (see Table 2). This result implied that individuals with relatively low values of R (i.e. 1.0 or 1.2) may not have exhibited maximum performance and, consequently, 25 full-trajectory trials from these individuals were excluded. These individuals did not produce any partial-trajectory trial.

For the six individuals that produced at least one full-trajectory trial and at least one partial-trajectory trial, F_{max}^* was estimated twice for each individual using either only full-trajectory trial(s) or only

Journal of Experimental Biology (2020) 223, jeb218552. doi:10.1242/jeb.218552

Table 2. Results from the bi-directional Student's *t*-tests comparing individual maximum force production in the different test groups

Compared groups (*N*)	$\overline{F^*_{max,1}}$	$\overline{F^*_{max,2}}$	*P*-value	d.f.
R=1.5 (15) and *R*=1.8 (6)	4.17	4.42	0.19	10
R=1.0 or 1.2 (4) and *R*=1.5 (15)	3.58	4.17	0.025	5
R=1.0 or 1.2 (4) and *R*=1.8 (6)	3.58	4.42	0.007	7
Full-trajectory trials (6) and partial-trajectory trials (6)	4.23	4.59	0.083	5
Non-QCA trials (13) and QCA trials (13)	3.86	4.43	<0.001	12

N, number of individual maximum performance data included; $\overline{F^*_{max,1}}$ $\overline{F^*_{max,2}}$, mean value of F^*_{max} for the compared groups (former and latter, respectively); d.f., degrees of freedom; *R*, loading ratio (globule mass/body mass, m_l/m_b); QCA, quasi-constant acceleration.

partial-trajectory trial(s). A paired bi-directional Student's *t*-test demonstrated that F^*_{max} from these two categories did not significantly differ (see Table 2), indicating that whether or not the start of the loaded fall trajectory was recorded did not affect the estimate of individual maximum force production.

Based on the 123 observations (96 full-trajectory trials and 27 partial-trajectory trials) for maximum force production from 26 individuals [*R*=1.5 (*N*=19) and *R*=1.8 (*N*=7)], the maximum value of individual maximum force production (F^*_{max}) for this set of individuals was 1.89×10^{-2} N (s.e.m. of 3.5×10^{-4} N), whereas the maximum F^*_{max} within the sample was 5.47 (s.e.m. of 0.157). Multiple observations of maximum vertical force were obtained for 23 dragonflies [*R*=1.5 (*N*=17) and *R*=1.8 (*N*=6)]. Weighting the F^*_{max} of these 23 individuals by their estimation errors, we then estimated maximum body weight-specific force production for the entire sample to be 4.27 (s.e.m. of 0.005).

After determining values of F_{max} for each of the aforementioned 26 individuals, log-transformed data were regressed against log-transformed body mass to evaluate the allometry of force production (Fig. 6). For the pooled dataset individuals, the ordinary least squares linear regression was significant ($\log F_{max}=0.86\log m_b-1.44$; $r^2=0.71$, $P<0.001$), with 95% CI for the slope between 0.64 and 1.07, indicating non-significant deviation from isometry.

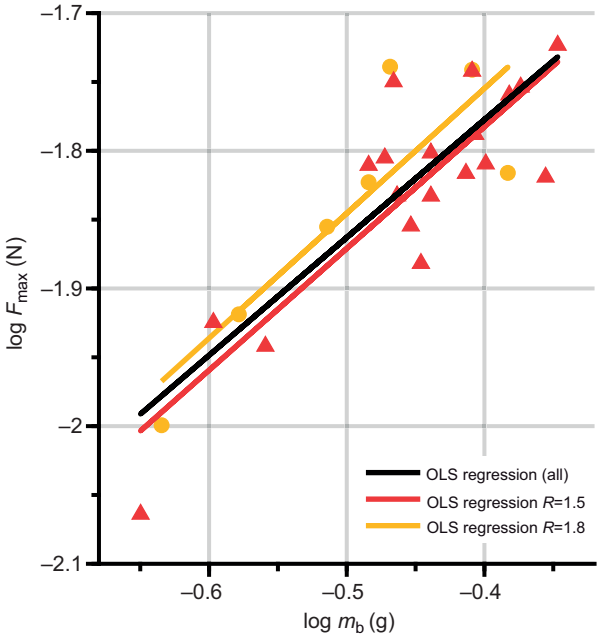

Fig. 6. Correlations between maximum force production and body mass for individual dragonflies. Data points for individuals with *R*=1.5 (the loading ratio, where $R=m_l/m_b$; *N*=19) are indicated by red triangles, whereas those for individuals with *R*=1.8 (*N*=7) are indicated by orange circles. Results of ordinary least squares linear regressions are as follows for log-transformed data: all individuals: $\log F_{max}=0.86\log m_b-1.44$ ($r^2=0.71$, $P<0.001$); individuals with *R*=1.5, $\log F_{max}=0.88\log m_b-1.43$ ($r^2=0.72$, $P<0.001$); individuals with *R*=1.8, $\log F_{max}=0.91\log m_b-1.39$ ($r^2=0.69$, $P<0.01$).

DISCUSSION

The method used here for eliciting maximum free-flight forces in dragonflies clearly indicates a capacity well exceeding that of steady trimmed flight, but identification of upper limits requires that (a) maximum performance during loaded falls and subsequent recovery were adequately assessed, and (b) the estimated maxima approximate absolute maximum capacities.

Relative to the first criterion, we establish that no large time-averaged force was exerted in the 30 trials for which the QCA method failed to yield maximum vertical accelerations. We can quantitatively evaluate an individual's performance in a single loaded fall trial via a recovery coefficient (C_r), a ratio indicating the extent to which a loaded dragonfly recovered from falling:

$$C_r = \frac{|w_{max} - w_{min}|}{|w_{min}|}, \quad (5)$$

where w_{min} is the dragonfly's minimum vertical velocity during the flight, and w_{max} is the maximum vertical velocity subsequently attained. The denominator corresponds to the dragonfly's maximum gain of downward speed, and the numerator corresponds to the maximum reduction in downward speed (plus the maximum accumulation of upward speed, if applicable). For all 178 recorded trials, values of C_r ranged from 0.09 to 1.78.

The 30 trials with no QCA period present, and thus with no observed maximum force production, are referred to as non-QCA trials; the other 148 trials with a QCA period present are referred to as QCA trials. Values of C_r for QCA trials ranged from 0.19 to 1.78, whereas values for non-QCA trials were all less than 0.67, indicating that the QCA method was sufficient for all trials with a C_r higher than 0.67. For non-QCA trials, the relatively low values of C_r suggest an inability to maintain large vertical force production over a sufficient period of time so as to gain enough positive vertical momentum. We also calculated, for all non-QCA trials, the time-averaged body weight-specific vertical forces produced during acceleration from w_{min} to w_{max}. Equating these values to maximum force production during flight, we obtained an estimate of F^*_{max} for 13 individuals. A paired bi-directional Student's *t*-test was then conducted to compare these F^*_{max} estimates with those estimates of the same individuals as determined from QCA trials; the former was significantly smaller than the latter, by a value of 0.57 (95% confidence interval: 0.31–0.84; see Table 2). Thus, non-QCA trials can be ignored as dragonflies did not maintain high aerodynamic forces during these flights.

Addressing the second criterion for identification of upper force limits, dragonflies generally extended the duration of vertical force production so as to achieve higher values of C_r, rather than increasing maximum forces per se. This result suggests that dragonflies were near their limits to force production in the recorded flights. For the 123 trials (96 full-trajectory trials and 27 partial-trajectory trials) used to determine group-level force production capacity, we obtained the time period *T* during which the dragonfly increased its vertical velocity from w_{min} to w_{max}, and investigated the relationship between *T* and C_r, and between F^*_V and C_r, respectively (Fig. 7). When C_r increased from 0.2 to 1.8, F^*_V

Journal of Experimental Biology (2020) 223, jeb218552. doi:10.1242/jeb.218552

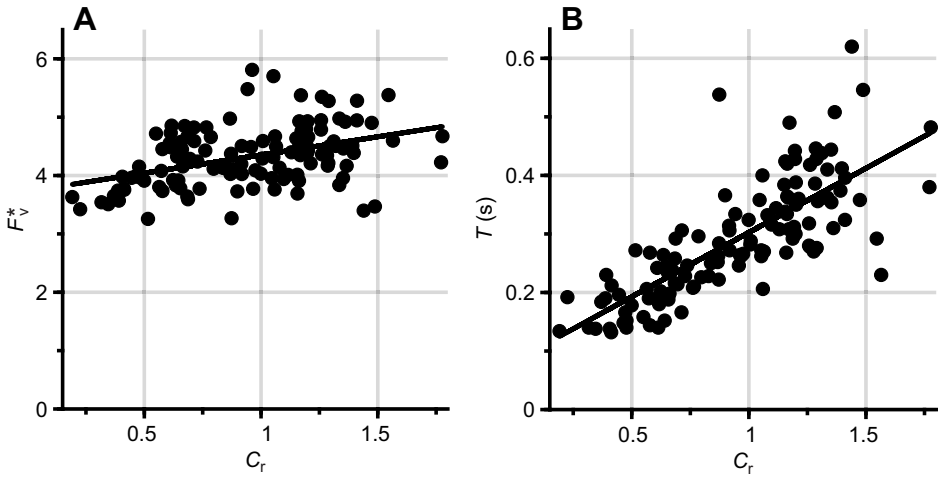

Fig. 7. Characterization of upper force limits. (A) Correlation between the maximum body weight-specific vertical forces (F^*_V) and the recovery coefficient (C_r). (B) Correlation between the time period (T) during which the dragonfly increased its vertical velocity from w_{min} to w_{max} and the recovery coefficient. Results of ordinary least squares linear regressions are as follows: (A) $F^*_V = 0.62C_r + 3.73$ (r^2=0.17, P<0.001); (B) T=0.22C_r+0.08 (r^2=0.60, P<0.001).

increased by 26% (from 3.85 to 4.85; see Fig. 7A), whereas T increased by 300% (from 0.12 s to 0.48 s; see Fig. 7B). With increasing C_r, the duration of force production thus increased 10 times more than did the magnitude of these forces, suggesting that the latter was close to an upper limit.

Estimated group-level capacity of the wandering glider suggests a time-averaged maximum vertical force of 4.27 times the body weight. This value is substantially higher than that reported for dragonflies in cumulative lifting of abdominally applied loads (i.e. 2.8; see Marden, 1987), and is comparable to transient estimates for free-flying dragonflies in various behavioral contexts (see Bomphrey et al., 2016; May, 1991; Rüppell, 1989; Lohmann et al., 2019). The value estimated here also well exceeds peak values for flapping cycle-averaged aerodynamic forces during voluntary maneuvers of dragonflies [e.g. 1.54 in turning flight (Li and Dong, 2017) and 1.33 in take-off (Li et al., 2018)]. Surprisingly, the value obtained here is much higher than the body weight-specific maximum force capacity reported for vertical load lifting by a range of other flying animals (some of which are of comparable body mass), including a value of 1.52 for bumblebees (Buchwald and Dudley, 2010), 1.8–2.1 for orchid bees (Dillon and Dudley, 2004), 2.2 for fruit flies (Lehmann, 1999), 2.26 for tree sparrows (Sun et al., 2016) and 1.8–3.9 for hummingbirds (Chai et al., 1997; Altshuler et al., 2010). These comparisons suggest that free forward flight with submaximal load may elicit behavioral responses different from those in vertical ascent, and that kinematic constraints identified in vertical and sustained load lifting (e.g. maximum stroke amplitude; see Dudley, 2000) may not pertain to the flight behaviors described here. Detailed high-speed assessment of wing motions would be necessary to assess this hypothesis. The results obtained for the wandering glider also indicated an isometric increase in total force production with increasing body size (Fig. 6), as opposed to negative allometries obtained in interspecific studies of asymptotic load lifting in orchid bees (Dillon and Dudley, 2004) and hummingbirds (Altshuler et al., 2010). Further assessment of intraspecific variation in morphological (e.g. relative muscle mass) and kinematic features (e.g. wingbeat frequency) during loaded flights of dragonflies would be informative in understanding these differing allometries.

In conclusion, we present a new method for assessing maximum force production by free-flying dragonflies, namely submaximally loaded falling, which elicits much higher whole-body forces than have previously been reported. Using a subset of trajectories for which accelerations were both high and sustained (i.e. using the QCA method), and by applying the Weibull distribution to better estimate population-level performance, we estimate maximum aerodynamic force production to be 4.3 times the body weight for this particular dragonfly species. With corresponding modification of the present method, consistent measurements of maximum force production during free flight could be obtained for various volant taxa, some of which have been studied relative to performance limits only in hovering flight using load-lifting methods. The method described here is also amenable to studying flight with ablated wings, and flight in variable-density gas mixtures.

Acknowledgements
We thank Yingxin Du, Wenqian Wu and Chengwang Zhang for assistance with experiments and data analysis, Yu Zeng for helpful comments, Victor M. Ortega-Jimenez for instructions on GCVSPL, and Travis J. Hagey for advice on Weibull distribution modeling.

Competing interests
The authors declare no competing or financial interests.

Author contributions
Conceptualization: G.S., R.D., T.P., Q.L.; Methodology: G.S., R.D., T.P., Q.L.; Software: G.S., M.Z., L.P.; Validation: G.S., M.Z., L.P.; Formal analysis: G.S., R.D., T.P., Q.L.; Investigation: G.S., M.Z., L.P.; Resources: G.S., R.D., T.P., M.Z., L.P., Q.L.; Data curation: G.S., T.P.; Writing - original draft: G.S., R.D., T.P.; Writing - review & editing: G.S., R.D., T.P., M.Z., L.P., Q.L.; Visualization: G.S., R.D., T.P.; Supervision: R.D., T.P., Q.L.; Project administration: G.S., R.D., T.P., M.Z., Q.L.; Funding acquisition: G.S., T.P., Q.L.

Funding
This work was supported by National Natural Science Foundation of China (grant nos 51636001 and 51706008), National Science and Technology Major Project (2017-II-0005-0018), and Aeronautics Power Foundation of China (grant no. 6141B090315). G.S. was funded by China Scholarship Council.

Data availability
Raw and smoothed time series of kinematic parameters, i.e. position, velocity and acceleration, for all loaded fall trials that were examined in the present study are available from the Dryad digital repository (Su et al., 2020): https://doi.org/10.6078/D1RQ57

Supplementary information
Supplementary information available online at
https://jeb.biologists.org/lookup/doi/10.1242/jeb.218552.supplemental

References
Altshuler, D. L., Dudley, R., Heredia, S. M. and McGuire, J. A. (2010). Allometry of hummingbird lifting performance. *J. Exp. Biol.* **213**, 725-734. doi:10.1242/jeb.037002

Anderson, R. C. (2009). Do dragonflies migrate across the western Indian Ocean? *J. Trop. Ecol.* **25**, 347-358. doi:10.1017/S0266467409006087
Bomphrey, R. J., Nakata, T., Henningsson, P. and Lin, H.-T. (2016). Flight of the dragonflies and damselflies. *Phil. Trans. R. Soc. B* **371**, 20150389. doi:10.1098/rstb.2015.0389
Buchwald, R. and Dudley, R. (2010). Limits to vertical force and power production in bumblebees (Hymenoptera: *Bombus impatiens*). *J. Exp. Biol.* **213**, 426-432. doi:10.1242/jeb.033563
Chai, P. and Dudley, R. (1995). Limits to vertebrate locomotor energetics suggested by hummingbirds hovering in heliox. *Nature* **377**, 722-725. doi:10.1038/377722a0
Chai, P. and Dudley, R. (1996). Limits to flight energetics of hummingbirds hovering in hypodense and hypoxic gas mixtures. *J. Exp. Biol.* **199**, 2285-2295.
Chai, P., Chen, J. S. and Dudley, R. (1997). Transient hovering performance of hummingbirds under conditions of maximal loading. *J. Exp. Biol.* **200**, 921-929.
Corbet, P. S. (2004). *Dragonflies: Behaviour and Ecology of Odonata*: Harley Books.
Dillon, M. E. and Dudley, R. (2004). Allometry of maximum vertical force production during hovering flight of neotropical orchid bees (Apidae: Euglossini). *J. Exp. Biol.* **207**, 417-425. doi:10.1242/jeb.00777
Dudley, R. (2000). *The Biomechanics of Insect Flight: Form, Function, Evolution*: Princeton University Press.
Hagey, T. J., Puthoff, J. B., Crandell, K. E., Autumn, K. and Harmon, L. J. (2016). Modeling observed animal performance using the Weibull distribution. *J. Exp. Biol.* **219**, 1603-1607. doi:10.1242/jeb.129940
Hagey, T. J., Uyeda, J. C., Crandell, K. E., Cheney, J. A., Autumn, K. and Harmon, L. J. (2017). Tempo and mode of performance evolution across multiple independent origins of adhesive toe pads in lizards. *Evolution* **71**, 2344-2358. doi:10.1111/evo.13318
Hedrick, T. L. (2008). Software techniques for two- and three-dimensional kinematic measurements of biological and biomimetic systems. *Bioinspir. Biomim.* **3**, 034001.
Lehmann, F.-O. (1999). Ambient temperature affects free-flight performance in the fruit fly Drosophila melanogaster. *J. Comp. Physiol. B* **169**, 165-171. doi:10.1007/s003600050207
Li, C. and Dong, H. (2017). Wing kinematics measurement and aerodynamics of a dragonfly in turning flight. *Bioinspir. Biomim.* **12**, 026001. doi:10.1088/1748-3190/aa5761
Li, Q., Zheng, M., Pan, T. and Su, G. (2018). Experimental and numerical investigation on dragonfly wing and body motion during voluntary take-off. *Sci. Rep.* **8**, 1011. doi:10.1038/s41598-018-19237-w
Lohmann, A. C., Corcoran, A. J. and Hedrick, T. L. (2019). Dragonflies use underdamped pursuit to chase conspecifics. *J. Exp. Biol.* **222**, jeb190884. doi:10.1242/jeb.190884
Marden, J. H. (1987). Maximum lift production during takeoff in flying animals. *J. Exp. Biol.* **130**, 235-258.
May, M. L. (1991). Dragonfly flight: power requirements at high speed and acceleration. *J. Exp. Biol.* **158**, 325-342.
Mountcastle, A. M. and Combes, S. A. (2013). Wing flexibility enhances load-lifting capacity in bumblebees. *Proc. R. Soc. B* **280**, 20130531. doi:10.1098/rspb.2013.0531
Plateau, F. A. J. (1865). Sur la force musculaire des insectes. *Bull. Acad. R. Belg. Cl. Sci.* **34**, 732-757.
Ray, R. P., Nakata, T., Henningsson, P. and Bomphrey, R. J. (2016). Enhanced flight performance by genetic manipulation of wing shape in *Drosophila*. *Nat. Commun.* **7**, 10851. doi:10.1038/ncomms10851
Rüppell, G. (1989). Kinematic analysis of symmetrical flight manoeuvres of Odonata. *J. Exp. Biol.* **144**, 13-42.
Su, G., Dudley, R., Pan, T., Zheng, M., Peng, L. and Li, Q. (2020). Data from: Maximum aerodynamic force production by the wandering glider dragonfly (Pantala flavescens, Libellulidae), v5, UC Berkeley. Dryad Dataset. doi:10.6078/D1RQ57
Sun, Y.-F., Ren, Z.-P., Wu, Y.-F., Lei, F.-M., Dudley, R. and Li, D.-M. (2016). Flying high: limits to flight performance by sparrows on the Qinghai-Tibet Plateau. *J. Exp. Biol.* **219**, 3642-3648. doi:10.1242/jeb.142216
Vance, J. T. and Roberts, S. P. (2014). The effects of artificial wing wear on the flight capacity of the honey bee *Apis mellifera*. *J. Insect Physiol.* **65**, 27-36. doi:10.1016/j.jinsphys.2014.04.003
Wakeling, J. and Ellington, C. (1997). Dragonfly flight. II. Velocities, accelerations and kinematics of flapping flight. *J. Exp. Biol.* **200**, 557-582.
Woltring, H. J. (1986). A Fortran package for generalized, cross-validatory spline smoothing and differentiation. *Adv. Eng. Software* **8**, 104-113. doi:10.1016/0141-1195(86)90098-7

1. Figures

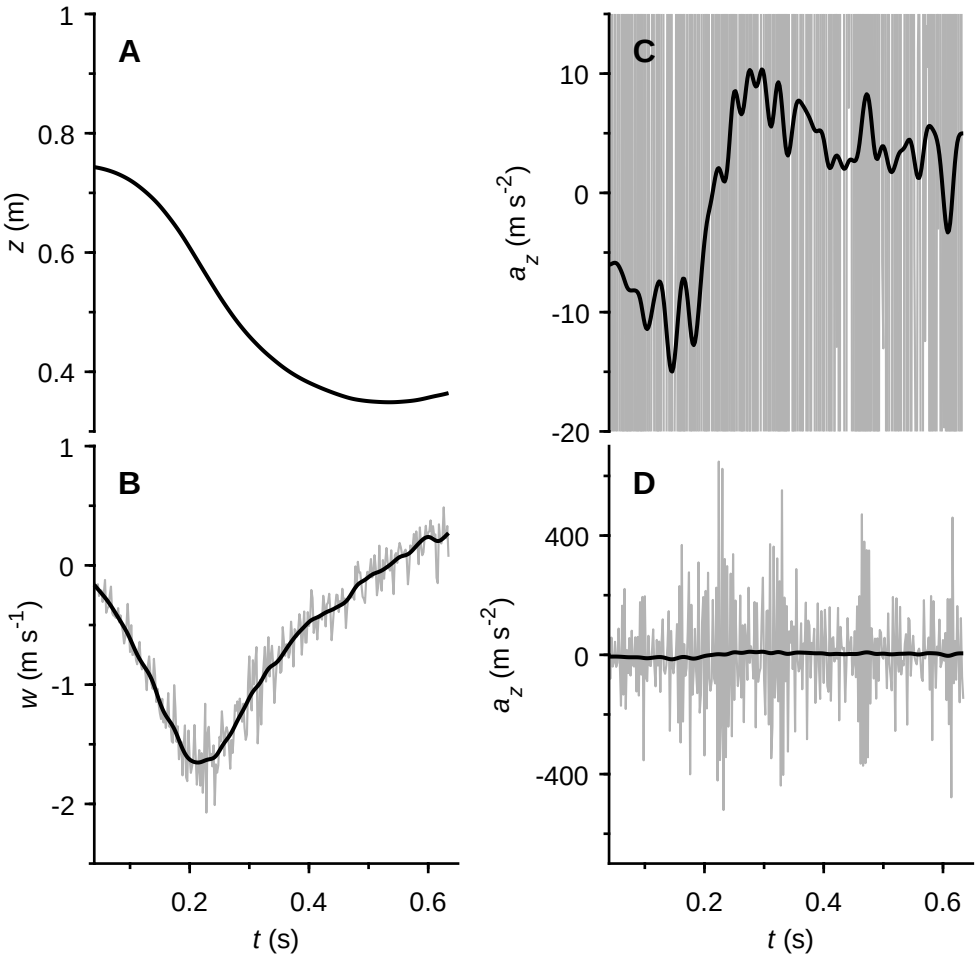

Fig. S1

Fig. S1. Kinematic parameters derived from raw and smoothed vertical position data for one loaded fall trial (trial index: 1808091348; preforming individual index: 180809-4). (A) raw and smoothed vertical position data (*z*, *Z*-position after release; *t*=0, time of release); (B) vertical velocity data derived from raw and smoothed vertical position data, respectively (*w*, *Z*-velocity after release); (C) vertical acceleration data derived from raw and smoothed vertical position data, respectively, with a smaller scale of a_z (a_z, *Z*-acceleration after release); (D) vertical acceleration data derived from raw and smoothed vertical position data, respectively, with a larger scale of a_z. In (A) to (D), thin gray line indicates raw positional data or kinematic data obtained by differentiating the raw positional data, thick black line indicates smoothed positional data or kinematic data obtained by differentiating the smoothed positional data. In (A), two lines almost overlap completely as the two set of positional data are close to each other. In (C), a smaller scale of a_z is used to clearly illustrate the thick black line. In (D), a larger scale of a_z is used to clearly illustrate the thin gray line.

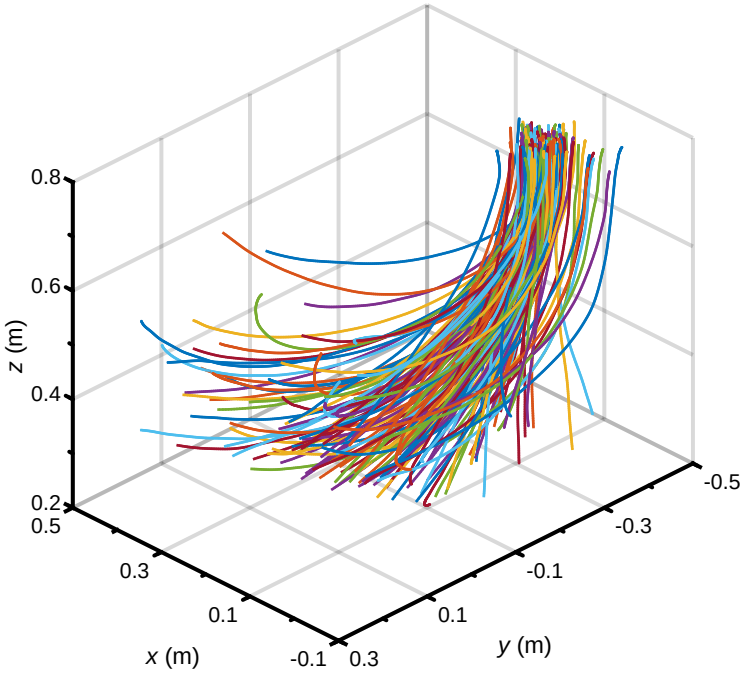

Fig. S2

Fig. S2. Three-dimensional flight trajectories tracked from 143 full-trajectory trials.

2. Tables

Table S1. Information for individual dragonflies: loading ratio (R), body mass (m_b), morphological data (l_b: body length; l_{fws}: forewing span length; l_{hws}: hindwing span length), force estimates (F_{max} and F^*_{max}), and number of QCA trials (N_{QCA}).

Individual index	R	m_b	l_b	l_{fws}	l_{hws}	$F_{max}\ (s.e.m.)$	$F^*_{max}\ (s.e.m.)$	N_{QCA}
180803-4	1.5	392	52	47	44	1.63	4.24	1
180803-5	1.5	253	53	47	44	1.19 (0.020)	4.80 (0.080)	11
180803-7	1.5	276	52	45	42	1.14 (0.020)	4.23 (0.072)	3
180804-4	1.5	352	n/a	n/a	n/a	1.40 (0.073)	4.05 (0.212)	5
180804-6	1.5	337	n/a	n/a	n/a	1.57 (0.070)	4.74 (0.213)	7
180804-7	1.5	342	n/a	n/a	n/a	1.78 (0.055)	5.31 (0.165)	5
180804-9	1.5	364	n/a	n/a	n/a	1.58 (0.025)	4.43 (0.070)	3
180804-10	1.5	386	n/a	n/a	n/a	1.53 (0.053)	4.03 (0.140)	8
180805-1	1.5	399	50	44	42	1.55 (0.037)	3.96 (0.096)	3
180805-2	1.5	390	n/a	n/a	n/a	1.81 (0.041)	4.74 (0.106)	2
180805-3	1.5	358	49	44	42.5	1.31 (0.074)	3.74 (0.211)	2
180805-4	1.5	344	50	46	44	1.47 (0.016)	4.36 (0.047)	12
180805-5	1.5	415	52	44	43	1.74 (0.043)	4.28 (0.107)	3
180805-6	1.5	364	51	42	40	1.47 (0.020)	4.12 (0.056)	10
180805-7	1.5	328	51	43	40.5	1.55 (0.077)	4.81 (0.240)	5
180805-10	1.5	224	49	43	40	0.86 (0.005)	3.93 (0.025)	4
180809-2	1.2	374	50	44	42.5	1.38(0.000)	3.77(0.127)	8
180809-4	1.8	328	48	43	40	1.50 (0.022)	4.68 (0.069)	8
180809-5	1.2	212	48	42	41	0.65(0.000)	3.12(0.020)	8
180809-7	1.5	450	50	43	41	1.89 (0.035)	4.29 (0.078)	6
180809-9	1.0	446	50	42	40.5	1.69(0.000)	3.87(0.048)	8
180809-10	1.5	423	50	42	40	1.76 (0.017)	4.25 (0.040)	2
180809-12	1.8	390	50	43	41	1.81 (0.027)	4.75 (0.071)	3
180810-1	1.8	232	49	40	38.5	1.00 (0.043)	4.40 (0.190)	3
180810-3	1.8	340	50	41	39.5	1.82 (0.052)	5.47 (0.157)	5
180810-4	1.8	264	50	42	40.5	1.21	4.66	1
180810-5	1.8	306	51	41	39.5	1.40 (0.011)	4.65 (0.037)	4
180810-7	1.8	414	51	43	40	1.53 (0.028)	3.76 (0.070)	6
180810-8	1.5	441	51	43	40	1.52	3.51	1
180810-9	1.2	443	50	42	40	1.54	3.56	1

Units: m_b, mg; l_b, l_{fws}, and l_{hws}, mm; F_{max} (s.e.m.), 10^{-2} N.

Table S2. Information for each recorded trial: categorical data, temporal data on the QCA period corresponding to the maximum force production (t_{QCAs}: starting time; t_{QCAe}: ending time), force estimates (F_V^*, F_H^*, F_V, F_H), time length of acceleration (T), and recovery coefficient (C_r).

Individual index	Trial index	Full-trajectory trial?	QCA trial?	t_{QCAs}	t_{QCAe}	F_V^*	F_H^*	F_V	F_H	T	C_r
180803-4	1808031719	no	no	n/a	n/a	n/a	n/a	n/a	n/a	n/a	0.322
180803-4	1808031722	no	yes	0.082	0.232	4.239	0.999	1.629	0.384	0.228	0.728
180803-5	1808031757	yes	yes	0.422	0.572	3.691	0.431	0.915	0.107	0.338	1.156
180803-5	1808031801	yes	yes	0.262	0.412	4.507	1.144	1.118	0.284	0.362	1.320
180803-5	1808031804	yes	yes	0.214	0.364	4.511	1.724	1.119	0.428	0.374	1.391
180803-5	1808031812	yes	yes	0.240	0.390	4.398	1.107	1.091	0.275	0.308	1.130
180803-5	1808031815	yes	yes	0.246	0.396	4.463	1.268	1.107	0.314	0.354	1.353
180803-5	1808031817	yes	yes	0.232	0.382	4.921	0.901	1.220	0.223	0.310	1.361
180803-5	1808031820	yes	yes	0.248	0.398	4.929	1.053	1.222	0.261	0.300	1.199
180803-5	1808031822	yes	yes	0.306	0.456	4.947	0.811	1.227	0.201	0.280	1.257
180803-5	1808031825	yes	yes	0.206	0.356	4.976	1.318	1.234	0.327	0.362	1.335
180803-5	1808031827	yes	yes	0.330	0.480	4.945	0.828	1.226	0.205	0.324	1.410
180803-5	1808031830	yes	yes	0.242	0.422	4.812	0.919	1.193	0.228	0.292	1.187
180803-7	1808031845	yes	no	n/a	n/a	n/a	n/a	n/a	n/a	n/a	0.386
180803-7	1808031848	no	no	n/a	n/a	n/a	n/a	n/a	n/a	n/a	0.376
180803-7	1808031850	no	yes	0.002	0.152	4.325	2.334	1.170	0.631	0.152	0.640
180803-7	1808031852	yes	no	n/a	n/a	n/a	n/a	n/a	n/a	n/a	0.319
180803-7	1808031855	yes	yes	0.220	0.370	4.002	2.460	1.083	0.666	0.166	0.472
180803-7	1808031857	no	yes	0.040	0.190	4.156	1.836	1.124	0.497	0.228	0.828
180803-7	1808031859	yes	no	n/a	n/a	n/a	n/a	n/a	n/a	n/a	0.266
180803-7	1808031902	no	no	n/a	n/a	n/a	n/a	n/a	n/a	n/a	0.525
180803-7	1808031904	no	no	n/a	n/a	n/a	n/a	n/a	n/a	n/a	0.668

180803-7	1808031906	no	no	n/a	n/a	n/a	n/a	n/a	n/a	n/a	0.120
180804-4	1808041504	yes	yes	0.294	0.444	3.838	0.601	1.324	0.207	0.410	1.335
180804-4	1808041522	no	yes	0.062	0.220	3.735	1.512	1.289	0.521	0.268	0.578
180804-4	1808041525	no	yes	0.080	0.230	4.598	1.063	1.586	0.367	0.230	1.565
180804-4	1808041527	yes	no	n/a	n/a	n/a	n/a	n/a	n/a	n/a	0.257
180804-4	1808041530	no	yes	0.044	0.308	3.257	1.246	1.124	0.430	0.272	0.516
180804-4	1808041533	no	yes	0.142	0.292	3.833	1.240	1.322	0.428	0.264	0.635
180804-6	1808041538	yes	yes	0.368	0.518	3.469	0.401	1.146	0.132	0.546	1.488
180804-6	1808041540	yes	yes	0.180	0.330	4.902	1.301	1.619	0.430	0.358	1.474
180804-6	1808041551	yes	no	n/a	n/a	n/a	n/a	n/a	n/a	n/a	0.398
180804-6	1808041554	yes	yes	0.232	0.390	5.282	1.023	1.745	0.338	0.396	1.411
180804-6	1808041557	yes	yes	0.218	0.394	3.399	0.669	1.123	0.221	0.620	1.440
180804-6	1808041600	yes	no	n/a	n/a	n/a	n/a	n/a	n/a	n/a	0.091
180804-6	1808041602	yes	yes	0.254	0.404	4.787	1.049	1.581	0.347	0.318	1.257
180804-6	1808041606	yes	yes	0.238	0.388	4.730	1.432	1.563	0.473	0.140	0.613
180804-6	1808041608	yes	yes	0.280	0.430	4.674	0.362	1.544	0.120	0.482	1.777
180804-6	1808041610	yes	no	n/a	n/a	n/a	n/a	n/a	n/a	n/a	0.486
180804-7	1808041616	no	yes	0.062	0.212	4.824	2.396	1.617	0.803	0.210	0.766
180804-7	1808041619	no	yes	0.062	0.212	4.975	1.437	1.668	0.482	0.252	0.867
180804-7	1808041636	no	yes	0.088	0.238	4.855	2.044	1.627	0.685	0.180	0.617
180804-7	1808041638	no	yes	0.110	0.260	5.703	1.100	1.912	0.369	0.262	1.053
180804-7	1808041639	no	yes	0.098	0.248	5.349	0.488	1.793	0.164	0.278	1.261
180804-9	1808041708	no	yes	0.080	0.230	4.484	1.522	1.600	0.543	0.192	0.614
180804-9	1808041710	no	yes	0.120	0.270	4.456	0.448	1.590	0.160	0.270	1.277
180804-9	1808041713	yes	yes	0.352	0.502	4.116	0.561	1.469	0.200	0.284	0.873
180804-10	1808041729	yes	yes	0.326	0.476	3.761	0.640	1.423	0.242	0.400	1.058

180804-10	1808041731	yes	yes	0.218	0.388	4.013	1.007	1.518	0.381	0.424	1.156
180804-10	1808041734	yes	no	n/a	n/a	n/a	n/a	n/a	n/a	n/a	0.543
180804-10	1808041737	yes	yes	0.276	0.426	4.622	0.548	1.749	0.207	0.268	1.160
180804-10	1808041739	yes	yes	0.310	0.460	3.594	0.833	1.360	0.315	0.292	0.687
180804-10	1808041741	yes	yes	0.338	0.488	3.728	0.735	1.410	0.278	0.366	0.898
180804-10	1808041743	yes	yes	0.234	0.384	3.774	1.349	1.428	0.510	0.132	0.412
180804-10	1808041745	yes	yes	0.312	0.462	3.774	0.927	1.428	0.351	0.246	0.737
180804-10	1808041747	yes	yes	0.264	0.466	3.782	1.437	1.431	0.544	0.234	0.654
180804-10	1808041749	yes	no	n/a	n/a	n/a	n/a	n/a	n/a	n/a	0.517
180805-2	1808051455	no	yes	0.088	0.238	4.823	1.466	1.844	0.560	0.166	0.712
180805-2	1808051457	no	yes	0.132	0.286	4.488	0.465	1.716	0.178	0.246	0.957
180805-2	1808051500	yes	no	n/a	n/a	n/a	n/a	n/a	n/a	n/a	0.554
180805-4	1808051509	yes	yes	0.210	0.376	4.198	0.840	1.415	0.283	0.314	0.915
180805-4	1808051512	yes	yes	0.184	0.334	4.166	0.876	1.405	0.295	0.508	1.367
180805-4	1808051515	yes	yes	0.192	0.342	4.169	1.415	1.406	0.477	0.446	1.286
180805-4	1808051518	yes	yes	0.216	0.394	4.363	1.110	1.471	0.374	0.418	1.261
180805-4	1808051522	yes	yes	0.214	0.430	4.387	0.546	1.479	0.184	0.412	1.397
180805-4	1808051524	yes	yes	0.228	0.378	4.453	1.209	1.501	0.408	0.144	0.577
180805-4	1808051527	yes	yes	0.270	0.420	4.591	0.615	1.548	0.207	0.288	1.008
180805-4	1808051529	yes	yes	0.330	0.480	4.349	0.775	1.466	0.261	0.362	1.168
180805-4	1808051531	yes	yes	0.268	0.432	3.957	1.005	1.334	0.339	0.444	1.351
180805-4	1808051533	yes	yes	0.302	0.452	4.345	0.545	1.465	0.184	0.386	1.283
180805-4	1808051535	yes	yes	0.300	0.450	4.208	0.423	1.419	0.142	0.360	1.212
180805-4	1808051536	yes	yes	0.302	0.452	4.213	0.794	1.421	0.268	0.428	1.288
180805-1	1808051546	yes	yes	0.240	0.390	4.027	1.352	1.575	0.529	0.262	0.869
180805-1	1808051548	yes	yes	0.342	0.494	4.026	1.065	1.574	0.416	0.272	0.918

180805-1	1808051553	yes	yes	0.214	0.364	3.542	1.476	1.385	0.577	0.140	0.316
180805-3	1808051559	yes	yes	0.272	0.430	3.268	1.466	1.147	0.514	0.538	0.874
180805-3	1808051604	yes	yes	0.262	0.412	3.916	1.351	1.374	0.474	0.244	0.646
180805-5	1808051614	yes	yes	0.240	0.390	3.979	2.338	1.619	0.951	0.138	0.406
180805-5	1808051616	yes	yes	0.222	0.372	4.428	1.959	1.801	0.797	0.208	0.761
180805-5	1808051618	yes	yes	0.232	0.382	4.152	2.230	1.689	0.907	0.152	0.478
180805-5	1808051621	yes	no	n/a	n/a	n/a	n/a	n/a	n/a	n/a	0.361
180805-6	1808051642	yes	yes	0.282	0.432	3.641	0.756	1.299	0.270	0.258	0.684
180805-6	1808051646	yes	yes	0.308	0.458	3.955	0.428	1.411	0.153	0.358	1.046
180805-6	1808051648	yes	yes	0.306	0.456	4.031	0.302	1.438	0.108	0.324	0.999
180805-6	1808051650	yes	yes	0.308	0.458	3.910	0.294	1.395	0.105	0.334	1.162
180805-6	1808051652	yes	yes	0.294	0.444	3.941	0.148	1.406	0.053	0.316	1.097
180805-6	1808051654	yes	yes	0.328	0.478	4.011	0.405	1.431	0.144	0.344	1.116
180805-6	1808051657	yes	yes	0.294	0.444	4.089	0.435	1.459	0.155	0.266	0.976
180805-6	1808051659	yes	yes	0.304	0.454	4.292	0.192	1.531	0.068	0.282	1.006
180805-6	1808051701	yes	yes	0.294	0.444	4.133	0.550	1.475	0.196	0.332	1.079
180805-6	1808051703	yes	yes	0.302	0.452	4.315	0.343	1.539	0.123	0.272	1.053
180805-7	1808051711	yes	yes	0.306	0.456	5.379	0.944	1.729	0.304	0.292	1.546
180805-7	1808051713	yes	yes	0.212	0.362	4.226	1.492	1.359	0.480	0.380	1.771
180805-7	1808051717	yes	yes	0.296	0.446	4.799	0.530	1.543	0.170	0.312	1.193
180805-7	1808051720	yes	yes	0.226	0.386	3.773	1.305	1.213	0.420	0.262	0.966
180805-7	1808051724	yes	yes	0.326	0.476	4.671	0.683	1.502	0.220	0.206	1.060
180805-10	1808051808	yes	yes	0.214	0.378	3.803	1.150	0.835	0.252	0.206	0.564
180805-10	1808051810	yes	yes	0.252	0.402	3.912	1.120	0.859	0.246	0.178	0.500
180805-10	1808051813	yes	yes	0.296	0.446	3.923	1.313	0.861	0.288	0.202	0.623
180805-10	1808051816	yes	yes	0.244	0.394	3.972	1.872	0.872	0.411	0.140	0.477

180809-4	1808091333	yes	yes	0.218	0.368	4.637	1.123	1.491	0.361	0.384	1.151
180809-4	1808091336	yes	yes	0.216	0.426	4.425	0.533	1.422	0.171	0.388	1.201
180809-4	1808091339	yes	yes	0.188	0.338	4.381	1.095	1.408	0.352	0.428	1.197
180809-4	1808091342	yes	yes	0.210	0.360	4.502	0.743	1.447	0.239	0.356	1.294
180809-4	1808091348	yes	yes	0.232	0.382	4.929	1.073	1.585	0.345	0.420	1.164
180809-4	1808091351	yes	yes	0.234	0.384	4.585	1.207	1.474	0.388	0.438	1.311
180809-4	1808091355	yes	yes	0.210	0.360	4.504	1.087	1.448	0.349	0.442	1.197
180809-4	1808091358	yes	yes	0.240	0.390	4.762	1.178	1.531	0.379	0.490	1.174
180809-2	1808091414	yes	yes	0.262	0.412	3.412	0.416	1.251	0.152	0.344	1.291
180809-2	1808091418	yes	yes	0.292	0.442	4.213	0.155	1.544	0.057	0.278	1.529
180809-2	1808091420	yes	yes	0.320	0.470	4.005	0.383	1.468	0.140	0.294	1.753
180809-2	1808091422	yes	yes	0.230	0.380	3.746	0.511	1.373	0.187	0.344	1.738
180809-2	1808091425	yes	yes	0.264	0.414	3.315	0.395	1.215	0.145	0.342	1.477
180809-2	1808091430	yes	yes	0.402	0.564	3.246	0.107	1.190	0.039	0.330	1.003
180809-2	1808091432	yes	yes	0.276	0.426	3.487	0.333	1.278	0.122	0.426	1.382
180809-2	1808091434	yes	yes	0.336	0.520	3.456	0.172	1.267	0.063	0.336	1.029
180809-5	1808091443	yes	yes	0.380	0.530	3.118	0.616	0.648	0.128	0.390	1.022
180809-5	1808091446	yes	yes	0.334	0.484	3.127	0.556	0.650	0.116	0.348	0.862
180809-5	1808091449	yes	yes	0.210	0.360	3.035	0.997	0.631	0.207	0.378	0.883
180809-5	1808091451	yes	yes	0.318	0.468	3.185	0.587	0.662	0.122	0.322	1.004
180809-5	1808091453	yes	yes	0.298	0.486	3.109	0.503	0.646	0.105	0.272	0.749
180809-5	1808091455	yes	yes	0.324	0.474	3.126	0.452	0.649	0.094	0.294	0.769
180809-5	1808091457	yes	yes	0.292	0.442	2.894	1.332	0.601	0.277	0.208	0.453
180809-5	1808091459	yes	yes	0.306	0.456	3.118	0.046	0.648	0.009	0.318	0.759
180809-7	1808091503	yes	no	n/a	n/a	n/a	n/a	n/a	n/a	n/a	0.175
180809-7	1808091505	yes	yes	0.276	0.426	4.497	0.637	1.983	0.281	0.270	1.064

180809-7	1808091508	yes	yes	0.292	0.442	4.117	1.340	1.816	0.591	0.226	0.797
180809-7	1808091510	yes	yes	0.302	0.452	4.373	0.644	1.929	0.284	0.222	0.871
180809-7	1808091517	yes	yes	0.266	0.416	3.991	2.536	1.761	1.118	0.148	0.465
180809-7	1808091519	yes	yes	0.290	0.440	4.079	1.673	1.799	0.738	0.190	0.573
180809-7	1808091521	yes	yes	0.264	0.414	4.130	1.281	1.822	0.565	0.250	0.838
180809-12	1808091600	yes	no	n/a	n/a	n/a	n/a	n/a	n/a	n/a	0.176
180809-12	1808091602	yes	no	n/a	n/a	n/a	n/a	n/a	n/a	n/a	0.206
180809-12	1808091604	no	yes	0.104	0.254	4.553	0.895	1.740	0.342	0.242	0.609
180809-12	1808091606	no	yes	0.110	0.260	4.660	0.549	1.781	0.210	0.296	0.785
180809-12	1808091608	no	yes	0.104	0.254	4.848	1.143	1.853	0.437	0.238	0.673
180809-9	1808091613	yes	yes	0.278	0.428	3.637	0.893	1.590	0.390	0.330	1.420
180809-9	1808091617	yes	yes	0.278	0.428	3.770	0.670	1.648	0.293	0.330	1.522
180809-9	1808091620	yes	yes	0.318	0.468	3.765	0.843	1.646	0.368	0.236	1.002
180809-9	1808091623	yes	yes	0.272	0.450	3.693	0.625	1.614	0.273	0.302	1.550
180809-9	1808091625	yes	yes	0.292	0.442	3.894	0.875	1.702	0.383	0.214	1.033
180809-9	1808091627	yes	yes	0.304	0.454	4.045	0.607	1.768	0.265	0.316	1.555
180809-9	1808091630	yes	yes	0.302	0.452	3.886	0.638	1.699	0.279	0.218	1.080
180809-9	1808091634	yes	yes	0.296	0.446	3.769	0.743	1.647	0.325	0.242	1.150
180809-10	1808091636	no	yes	0.100	0.274	4.156	1.384	1.723	0.574	0.240	0.665
180809-10	1808091639	no	yes	0.110	0.260	4.285	1.208	1.777	0.501	0.214	0.695
180810-5	1808101503	yes	no	n/a	n/a	n/a	n/a	n/a	n/a	n/a	0.356
180810-5	1808101510	no	yes	0.168	0.318	4.509	0.357	1.352	0.107	0.364	1.164
180810-5	1808101513	yes	yes	0.216	0.366	4.718	1.554	1.415	0.466	0.158	0.550
180810-5	1808101516	yes	yes	0.238	0.388	4.576	1.668	1.372	0.500	0.188	0.657
180810-5	1808101518	yes	yes	0.288	0.438	4.658	1.499	1.397	0.449	0.216	0.684
180810-1	1808101533	yes	yes	0.244	0.394	4.448	1.367	1.011	0.311	0.198	0.661

180810-1	1808101537	yes	no	n/a	n/a	n/a	n/a	n/a	n/a	n/a	0.446
180810-1	1808101541	yes	no	n/a	n/a	n/a	n/a	n/a	n/a	n/a	0.417
180810-1	1808101543	yes	yes	0.204	0.354	3.631	2.028	0.826	0.461	0.134	0.191
180810-1	1808101545	yes	no	n/a	n/a	n/a	n/a	n/a	n/a	n/a	0.253
180810-1	1808101547	no	yes	0.128	0.278	4.590	0.987	1.044	0.224	0.306	0.714
180810-3	1808101604	no	yes	0.148	0.298	5.811	1.173	1.936	0.391	0.264	0.962
180810-3	1808101607	no	yes	0.160	0.310	5.480	1.108	1.826	0.369	0.334	0.942
180810-3	1808101610	no	yes	0.056	0.206	5.277	0.601	1.759	0.200	0.276	1.290
180810-3	1808101612	yes	yes	0.310	0.460	4.506	0.840	1.502	0.280	0.306	0.917
180810-3	1808101616	yes	no	n/a	n/a	n/a	n/a	n/a	n/a	n/a	0.253
180810-3	1808101618	no	yes	0.154	0.304	5.375	0.551	1.791	0.184	0.308	1.171
180810-3	1808101625	yes	no	n/a	n/a	n/a	n/a	n/a	n/a	n/a	0.203
180810-3	1808101627	no	no	n/a	n/a	n/a	n/a	n/a	n/a	n/a	0.623
180810-3	1808101629	no	no	n/a	n/a	n/a	n/a	n/a	n/a	n/a	0.476
180810-4	1808101632	yes	yes	0.296	0.446	4.659	0.920	1.206	0.238	0.350	1.202
180810-7	1808101650	yes	no	n/a	n/a	n/a	n/a	n/a	n/a	n/a	0.153
180810-7	1808101653	yes	yes	0.262	0.422	3.742	0.730	1.518	0.296	0.190	0.387
180810-7	1808101655	yes	yes	0.234	0.384	3.961	1.462	1.607	0.593	0.196	0.445
180810-7	1808101657	yes	yes	0.232	0.422	3.650	1.120	1.481	0.455	0.184	0.370
180810-7	1808101700	yes	yes	0.242	0.392	3.570	1.397	1.449	0.567	0.230	0.391
180810-7	1808101703	yes	yes	0.226	0.422	3.756	0.963	1.524	0.391	0.212	0.414
180810-7	1808101705	yes	no	n/a	n/a	n/a	n/a	n/a	n/a	n/a	0.340
180810-7	1808101708	no	no	n/a	n/a	n/a	n/a	n/a	n/a	n/a	0.371
180810-7	1808101709	yes	yes	0.262	0.412	3.422	0.913	1.389	0.370	0.192	0.225
180810-9	1808101721	yes	yes	0.320	0.470	3.558	0.323	1.545	0.140	0.306	1.089
180810-8	1808101730	yes	yes	0.304	0.454	3.509	1.653	1.517	0.715	0.138	0.345

Units: t_{QCAs}, t_{QCAe}, and T, s; F_V and F_H, 10^{-2} N.

3. Movies

Movie 1. Raw video from one camera view for one loaded fall trial (trial index: 1808091348; preforming individual index: 180809-4).

Movie 2. Raw video from the other camera view for one loaded fall trial (trial index: 1808091348; preforming individual index: 180809-4).